Estimating SERS Properties of Silver-Particle Aggregates through Generalized Mie Theory

Hongxing Xu[1,2] and Mikael Käll[3]

[1] Institute of Physics, Chinese Academy of Sciences, P.O. Box 603-146, Beijing, 100080, P. R. China
[2] Division of Solid State Physics, Lund University, Box 118, 221 00, Lund, Sweden
[3] Applied Physics, Chalmers University of Technology, 412 96, Göteborg, Sweden
kall@fy.chalmers.se

1 Introduction

It has long been known that the classical electromagnetic (em) enhancement mechanism is by far the most important contributor to SERS and related surface-enhanced spectroscopies [1]. The em theory provides a quantitative understanding of all the principal characteristics of SERS, including variation in enhancement with wavelength, polarization, nanostructure morphology and type of metal. When applied to aggregates of particles, it also makes it understandable why SERS can provide single-molecule sensitivity [2, 3]. Unfortunately, realistic estimates of em enhancement effects in nanostructured materials are in general not straightforward and invariably involves approximations. In this Chapter, we briefly summarize our recent work on em-enhancement phenomena in nanoparticle aggregates, focusing on theoretical results obtained through generalized Mie theory [2, 3, 4, 5, 6, 7, 8, 9, 10, 11]. The fundamental approximation of the model is thus that the metal nanoparticles are treated as spheres. Although this might be seen as a gross oversimplification, the advantage of the Mie approach is that it provides a complete and analytic solution to the full Maxwell's equations, including, for example, retardation effects. The Chapter is organized as follows: After introducing the basic elements of the em enhancement effect and generalized Mie theory (GMT), we briefly summarize the calculation technique in Sect. 2. Section 3 then discusses the main theory results, focusing on the concept of "hot sites" in nanoparticle junctions, their polarization dependence and the relation to far-field optical properties. We also briefly bring up the importance of optical forces in SERS and an extension of the em SERS theory that includes a quantum optical treatment of the molecular response.

1.1 Electromagnetic Enhancement

Consider a molecule located at a point $\boldsymbol{r}$ in the vicinity of a nanostructure and let the molecule–nanostructure system be illuminated by an external incident field $\boldsymbol{E}_{\mathrm{i}}$ with wavevector $\boldsymbol{k}$. Because of the electromagnetic response of the system, the local field $\boldsymbol{E}_{\mathrm{l}}$ at $\boldsymbol{r}$ will be different from $\boldsymbol{E}_{\mathrm{i}}$ by a factor

K. Kneipp, M. Moskovits, H. Kneipp (Eds.): Surface-Enhanced Raman Scattering – Physics and Applications, Topics Appl. Phys. **103**, 87–104 (2006)

$M = |\boldsymbol{E}_\mathrm{l}|/|\boldsymbol{E}_\mathrm{i}|$. This field-enhancement factor can be above or below unity, and its magnitude will be largest if the system supports internal electromagnetic resonances at the illumination frequency ω_0. The local field will induce a dipole moment in the molecule, and part of the molecular dipole scattering will appear at Raman-shifted frequencies $\omega_0 \pm \omega_\mathrm{vib}$. Because of electromagnetic reciprocity, that part of the dipole far-field that scatters into the $-\boldsymbol{k}$ direction and has the same polarization as the incident field will also be enhanced by the factor M, although the factor should now be evaluated at the Raman-shifted frequency of interest. Hence, the effective molecular Raman polarizability will be enhanced by a factor M^2 and the effective Raman cross section by a factor M^4. This power-of-four dependence makes it understandable why SERS is such a pronounced effect – even relatively modest field-enhancement factors, of the order 10–30, result in a huge Raman enhancement of the order $\sim 10^4$ to $\sim 10^6$. Similar types of arguments can be applied also to other types of surface-enhanced spectroscopies. In the case of fluorescence, the M^4 factor has to be multiplied by a factor $1/M_\mathrm{d}^2$, which compensates for the enhancement of the excited-state decay rate. If the fluorophore is far from the metal surface, we have that $M_\mathrm{d} \approx M$, which implies that the effective fluorescence cross section scales as M^2. For shorter distances (a few nanometers), $M_\mathrm{d} \gg M$ in general, and the fluorescence is quenched [9, 10, 11].

As noted above, a large field-enhancement factor requires some kind of electromagnetic resonance in the nanostructure, the most efficient and well known being localized surface plasmons (LSPs) of various types. This explains why silver, which can support sharp LSP modes over the entire visible to near-infrared wavelength range, and gold, which is useful at frequencies below the interband region ($\lambda >\sim 550\,\mathrm{nm}$), are the optimal materials for construction of SERS-active nanostructures. However, other kinds of resonances, for example diffractive modes in particle arrays or other types of spatially extended nanostructures, and purely electrostatic effects, such as the lightning-rod effect, can also contribute substantially to the field-enhancement factor. Naturally, the largest SERS signal is expected when several types of electrodynamic and electrostatic enhancement effects work in unison. This is the case in the single-molecule SERS experiments illustrated in Fig. 1 [2]. Here, hemoglobin (Hb) was incubated together with a heterogeneous Ag colloidal solution in a ratio of approximately one protein molecule per three Ag nanoparticles. The proteins, together with a low concentration of NaCl, cause a slight aggregation of the colloid, resulting in the formation of particle dimers and a few larger clusters. These small aggregates turned out to be highly SERS active, whereas the single isolated particles did not produce any measurable signal. Moreover, the Raman signal was maximal for dimers that were oriented parallel to the incident polarization, for which the SERS enhancement factor was experimentally estimated to be of the order 10^{10}. As will be discussed below, these observations can be understood from general-

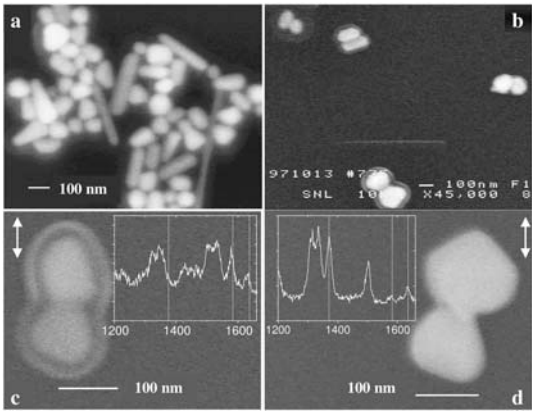

Fig. 1. (Reproduced from [2]), SEM images of immobilized Ag-particles. The pictures show (**a**) overview of Ag-particle shapes and sizes, (**b**) Ag-particle dimers observed after incubation with hemoglobin, and (**c**), (**d**) hot dimers and corresponding single-molecule Raman spectra. The *double arrows* in (**c**) and (**d**) indicate the polarization of the incident laser field

ized Mie theory (GMT) calculations of field-enhancement factors in the gap between Ag nanoparticles [2, 3].

1.2 Generalized Mie Theory

Mie theory [12] is a method to solve the boundary condition problem involved in the scattering and extinction of light by a single sphere situated in a homogeneous medium. This can be done through an expansion of the incident and scattered fields into vector spherical harmonics (VSHs). Mie theory has formed the basis for a vast range of techniques that can also be used to understand more complex scattering problems, for example a sphere above a flat surface, spheres composed of multiple concentric shells and ensembles of interacting spheres, which is the focus of the present chapter. Although any formal definition seems meaningless, we group these methods under a common heading, i.e., generalized Mie theory (GMT). Many of the GMT methods have proved instrumental for the development of a theoretical basis for surface-enhanced spectroscopy, plasmonics, and nano-optics in general. GMT also provides a convenient analytical comparison for a range of more novel grid-based methods in computational electromagnetics, such as the discrete dipole approximation (DDA) and the finite difference time-domain (FTDT) methods. Pioneering Mie theory contributions on SERS from aggregates include those of [13, 14, 15, 16, 17, 18].

A crucial component of GMT is the transition matrix (T-matrix) technique, introduced by *Waterman* [19, 20]. The T-matrix can be used to relate the VSH expansion coefficients for different spheres in an ensemble based on

the addition theorem of *Stein* [21] and *Cruzan* [22] and the total scattered field can then be obtained directly by solving a linear system of equations [23]. Various techniques to calculate the T-matrix of multisphere systems have been reported [20, 23, 24]. However, many of these methods are tedious when the distances between spheres are small or when the number of spheres is large. A complementary approach is the order-of-scattering (OS) method, which expresses the total scattered field from an ensemble as a sum of different scattering orders. By tracing the light paths in the multiple scattering processes, the contribution to the total field from each scattering event can be obtained by applying the boundary conditions for each single scatterer. *Fuller* has given the solution for the case of two spheres [25]. Recently, we developed a technique to calculate the scattering from multisphere systems using a recursive OS approach [7, 8]. This method is described briefly in the following paragraph.

2 The Recursive Order-of-Scattering Method

Similar to the original Mie theory [12], the incident electric field and the scattered electric field of an ensemble of L spheres are expanded in vector spherical harmonics (VSHs) as:

$$
\begin{aligned}
{}^{\mathrm{i}}\boldsymbol{E}_{\mathrm{l}} &= \sum_{n=1}^{\infty}\sum_{m=-n}^{n}\sum_{p=1}^{2} {}^{\mathrm{i}}C_{mnp}^{l}\,|mn1p\rangle \\
{}^{\mathrm{s}}\boldsymbol{E} &= \sum_{l=1}^{\oplus L} {}^{\mathrm{s}}\boldsymbol{E}_{\mathrm{l}} = \sum_{l=1}^{\oplus L}\sum_{n=1}^{\infty}\sum_{m=-n}^{n}\sum_{p=1}^{2} {}^{\mathrm{s}}C_{mnp}^{l}\,|mn3p\rangle,
\end{aligned}
\tag{1}
$$

where ${}^{\mathrm{i}}C_{mnp}^{l}$ and ${}^{\mathrm{s}}C_{mnp}^{l}$ are the expansion coefficients for the VSH $|mnjp\rangle$ centered at the l-th sphere, with $p = 1$ for $\boldsymbol{M}_{mn}^{j}$ and $p = 2$ for $\boldsymbol{N}_{mn}^{j}$, respectively. The index $j = 1, 2, 3, 4$ corresponds to spherical Bessel and Hankel functions j_n, y_n, $h_n^{(1)}$, $h_n^{(2)}$, respectively [26], and the symbol $\oplus$ means that the sum should be performed in Cartesian coordinates. The scattering coefficients ${}^{\mathrm{s}}C_{mnp}^{l}$ are functions of the incident coefficients ${}^{\mathrm{i}}C_{mnp}^{l}$, the corresponding Lorenz–Mie coefficients a_n^l and b_n^l, and the translation coefficients ${}^{lh}A_{mn}^{\mu\nu}$ and ${}^{lh}B_{mn}^{\mu\nu}$, relating sphere l to sphere h [21, 22], i.e:

$$
{}^{\mathrm{s}}C_{mnp}^{l} = {}^{L}\,T_l({}^{\mathrm{i}}C_{\mu\nu q}^{h}, a_\nu^h, b_\nu^h, {}^{lh}A_{mn}^{\mu\nu}, {}^{lh}B_{mn}^{\mu\nu})\,. \tag{2}
$$

Similarly, the corresponding magnetic fields can be expanded as:

$$
\begin{aligned}
\boldsymbol{H}_{\mathrm{i}}^{l} &= \frac{k}{i\omega\mu}\sum_{n=1}^{\infty}\sum_{m=-n}^{n}\sum_{p=1\neq p'}^{2} {}^{\mathrm{i}}C_{mnp}^{l}\,|mn1p'\rangle \\
\boldsymbol{H}_{\mathrm{s}} &= \frac{k}{i\omega\mu}\sum_{l=1}^{\oplus L}\boldsymbol{H}_{\mathrm{s}}^{l} = \frac{k}{i\omega\mu}\sum_{l=1}^{\oplus L}\sum_{n=1}^{\infty}\sum_{m=-n}^{n}\sum_{p=1\neq p'}^{2} {}^{\mathrm{s}}C_{mnp}^{l}\,|mn3p'\rangle
\end{aligned}
\tag{3}
$$

due to the relations $\boldsymbol{H} = \frac{1}{i\omega\mu}\nabla \times \boldsymbol{E}$, $\boldsymbol{N} = \frac{1}{k}\nabla \times \boldsymbol{M}$, $\boldsymbol{M} = \frac{1}{k}\nabla \times \boldsymbol{N}$.

The recursive OS method utilizes a matrix representation of T in (2), which is described as a product of the matrices G, which contain the expansion coefficients of the incident field for each sphere, and the response matrix Ψ of the L-sphere system, which transfer the incident coefficients to the scattering coefficients (for details see [8]). One can thus write

$$[{}^{L}T_1, {}^{L}T_2, {}^{L}T_3 \cdots {}^{L}T_L] = [G_1, G_2, G_3 \cdots G_L]\Psi^{(L)}\,, \tag{4}$$

where

$$\begin{aligned}
\Psi_{LL}^{(L)} &= S_L \sum_{i=0}^{N_{\mathrm{os}}} (\Omega^{(L-1)}\Psi^{(L-1)}\Omega'^{(L-1)}S_L)\,, \\
\Psi_{pL}^{(L)} &= \sum_{j=1}^{L-1} \Psi_{pj}^{(L-1)}\Omega_{j,L}\Psi_{LL}^{(L)} && p = 1, \ldots, L-1\,, \\
\Psi_{Lq}^{(L)} &= \Psi_{LL}^{(L)} \sum_{j=1}^{L-1} \Omega_{L,j}\Psi_{jq}^{(L-1)} && q = 1, \ldots, L-1\,, \\
\Psi_{pq}^{(L)} &= \Psi_{pq}^{(L-1)} + \Psi_{pL}^{(L)} \sum_{j=1}^{L-1} \Omega_{L,j}\Psi_{jq}^{(L-1)} && p, q = 1, \ldots, L-1\,.
\end{aligned} \tag{5}$$

Here, Ω_{pq} are matrices that contain the transfer coefficients relating VSHs originating in the p-th sphere to those originating in the q-th sphere, S_p are the matrices that contain the Mie scattering coefficients, while $\Omega^{(L-1)} = [\Omega_{L1}, \Omega_{L2}, \ldots, \Omega_{L,L-1}]$ and $\Omega'^{(L-1)} = [\Omega_{L1}, \Omega_{L2}, \ldots, \Omega_{L,L-1}]^T$ [8]. Moreover, it can be shown that the summation over different scattering orders $i \in [0, N_{\mathrm{OS}}]$ up to infinite order can be obtained through matrix inversion instead of summation, according to:

$$\begin{aligned}
\lim_{N_{\mathrm{OS}} \Rightarrow \infty} \sum_{i=0}^{N_{\mathrm{os}}} (\Omega^{(L-1)}\Psi^{(L-1)}\Omega'^{(L-1)}S_L) \\
= \frac{1}{1 - \Omega^{(L-1)}\Psi^{(L-1)}\Omega'^{(L-1)}S_L}\,.
\end{aligned} \tag{6}$$

In order to find the response matrix $\Psi^{(L)}$ for L spheres, we first find the response matrix $\Psi^{(L-1)}$ for $(L-1)$ spheres, and so on. Finally, the response matrix for the first sphere is found as $\Psi^{(1)} = S_1$. Using this recursive method, the response matrix $\Psi^{(L)}$ of L-spheres can be obtained according to (1)–(6).

Scattering problems that involve an arbitrary number of interacting spheres can in principle be solved exactly by the technique described briefly above. In practice, however, one needs to calculate a very large number of complex functions and translation coefficients that include a large number of multipoles n in order to ensure convergence, in particular for closely

spaced particles. If we let n range from 1 to N, the total number of VSHs will be $N \times (2N + 1) \times 2 \times 2$ for a two-sphere system, i.e., more than eighty thousand for $N = 100$. The total number of translation coefficients will be $\left[N \times (2N + 1) \times 2 \times 2\right]^2$, i.e., more than 6 billion. Moreover, if we have L spheres, the number of translation coefficients increases to $\frac{L}{2}(L-1) \times \left[N \times (2N + 1) \times 2 \times 2\right]^2$. Considering the complexity of calculating each translation coefficient, it is not surprising that GMT calculations of strongly interacting particles has turned out to be a challenge, both in terms of mathematical methodology and the computer capacity needed.

3 Examples of GMT Calculations for Ag-Particle Aggregates

3.1 "Hot Sites" Between Metal Particles

Figure 2 illustrates the effect of aggregation of metal particles in SERS. Using GMT, we have calculated the local field at two positions around two large (diameter $D = 200\,\text{nm}$) silver spheres separated by a gap of length d. The two spheres are illuminated by a plane wave polarized parallel to the dimer axis. For position A, located 0.5 nm from one of the spheres along the dimer axis, the factor M^4 increases dramatically for decreasing interparticle distances and reaches $\sim 10^9$ for $d = 1\,\text{nm}$. At position B, which is located 0.5 nm from the surface in the direction perpendicular to the dimer axis, there is no substantial enhancement at any separation. These effects can, in fact, be well accounted for by a simple electrostatic model. Imagine that the two particles were perfectly conducting and situated in a uniform electrostatic field E_i oriented in the direction of the dimer axis. Since the field will be excluded from the perfectly conducting spheres, the electrostatic potential drop will be concentrated to the interparticle region. From the geometry of the problem, this results in a local field between the spheres of strength $E_\text{l} = E_\text{i}(D + d)/d$. A molecule situated between the particles thus experiences a SERS enhancement factor of the order $M^4 = (D/d + 1)^4$, while molecules outside the interparticle region will experience no net enhancement ($M^4 \equiv 1$). The comparison between the simple electrostatic model and the full electrodynamic calculation in Fig. 2 clearly shows that the former captures much of the essential physics of the interparticle coupling problem.

Figure 3 illustrates the wavelength dependence of the SERS enhancement for dimers composed of identical Ag spheres of varying diameter D but with a fixed surface-to-surface separation $d = 1\,\text{nm}$. The prominent peaks that are evident in those spectra originate in plasmon modes of the dimer system. In particular, the longest-wavelength peak in each spectrum can be assigned to a mode dominated by the dipolar plasmons of each sphere coupled in phase. This mode has recently been identified in scattering spectra of nanofabricated Ag-particle dimers, and its dispersion with d and D has been shown

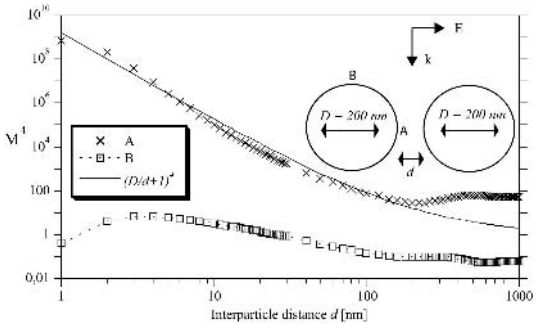

Fig. 2. (Adapted from [4]), Illustration of SERS enhancement, approximated as the fourth power of the field enhancement factor M, at two positions around a pair of silver spheres of diameter $D = 200\,\text{nm}$ for varying surface-to-surface separation d. The wavelength is $\lambda = 514.5\,\text{nm}$ and dielectric data for silver from [27] have been used in the GMT calculations. The *thin solid line* shows the electrostatic estimate of the enhancement effect. Note the logarithmic scales

to be in good agreement with electrodynamic calculations [28]. However, the prominence of the coupled dipole mode in the spectra of Fig. 3 does not imply that the field-enhancement effects can be understood within the dipole approximation. On the contrary, in order to build up the electrostatic component of the field enhancement between particles, a large number of multipolar resonances have to be taken into account. This is illustrated in Fig. 4, which shows the intensity enhancement factor M^2 versus the number of multipoles N used in a GMT calculation for a dimer of $D = 90\,\text{nm}$ spheres excited with light polarized parallel to the dimer axis. We see that for a separation distance of around $d = 10\,\text{nm}$, it is necessary to include multipoles up to order $N = 10$ whereas for distances down to 1 nm more than 50 multipolar terms are needed to reach convergence. The latter d value is probably close to the smallest interparticle distance for which classical electrodynamic calculations can be trusted. For even smaller separations, one approaches the spill-out region of the Ag s electrons [29], which should lead to interparticle currents that reduce the field strength in the gap region. Moreover, for smaller distances or for gaps between sharper structures, the nonlocal dielectric response of the metal has to be taken into account. Nonlocal effects can be expected to reduce the contribution from high-order multipoles [30], although to what extent is a matter of debate.

From GMT calculations such as those in Fig. 2 and Fig. 3, we find that the maximum SERS enhancement factor M^4 at "hot sites", i.e., in gaps, in Ag-dimer systems peaks at around 10^{11} to 10^{12} for gap distances of the order 1 nm. Taking into account the Stokes shift in the Raman process and the possibility that the imaginary part of the Ag dielectric function may be larger than in the experimental values used [27], a more conservative value for the maximum em SERS enhancement might be 10^{10}. Although no formal proof

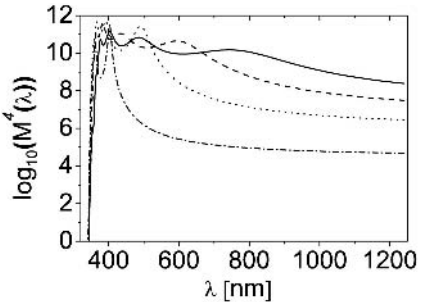

Fig. 3. (Adapted from [3]), SERS enhancement factor M^4 as function of wavelength for the midpoint between two identical Ag spheres with surface-to-surface separation $d = 1$ nm and different diameters: $D = 140$ nm, 100 nm, 60 nm and 20 nm, from *top* to *bottom*. The dimer is illuminated with light polarized parallel to the dimer axis and with incident $\boldsymbol{k}$ vector normal to this axis

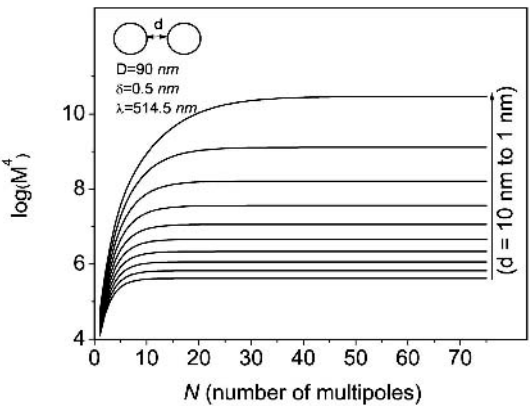

Fig. 4. (Adapted from [4]), Calculated intensity enhancement M^2 for a position along the dimer axis 0.5 nm from the surface of one of the spheres as a function of the number of multipoles N included in the GMT calculation. The diameters of the spheres are 90 nm, and the incident polarization is parallel to the dimer axis. The calculations are performed for different surface-to-surface distances d, from 1 nm to 10 nm

exists, it seems likely that this is also close to the maximum em enhancement factor in any type of Ag or Au nanostructure that contains gaps or crevices of similar dimensions.

3.2 Polarization Anisotropy

From the GMT results above, we have seen that the SERS enhancement in small nanoparticle aggregates is expected to be a highly localized phenomenon. Due to the combination of electrostatic effects and electrodynamic LSP modes, the calculated M^4 factor can reach above 10^{10} in the gap regions between particles, and at the same time be at or below unity outside these areas. The gaps between particles thus constitute "hot sites" for SERS and the molecules at those sites are expected to dominate the net SERS signal

from an aggregate, even if the whole aggregate is covered by molecules. However, the gap regions are not "hot" for all incident polarizations. If a dimer is excited with light polarized perpendicular to the dimer axis, the field is instead excluded from the gap region, resulting in an enhancement below unity. We thus expect the SERS signal from dimers and other small aggregates to be highly polarization dependent. Figure 5 gives an experimental example that illustrates this effect. The samples in this study were prepared in a similar way to the ones in Fig. 1, i.e., by first incubating hemoglobin and colloidal Ag particles and then immobilizing the resulting Hb/Ag aggregates for Raman and electron microscopy investigations. However, the Hb:Ag-particle ratio was $\sim$ 100 times higher in the present case. Figure 5a shows a SEM image of a number of Hb/Ag aggregates within one investigated area. The corresponding polarized Raman images for different angles between the incident polarization and the coordinate system of the sample are shown in Fig. 5b. Six bright spots, marked as A to F, could be clearly identified as different aggregates in the SEM, and the intensities of these spots varied to different degrees with the incident polarization. Figure 5c shows a polar plot of this variation for spot A, which turned out to be a dimer with its dimer axis rotated $\alpha_0 \approx 125°$ relative to the vertical axis in Fig. 5a. It is clear that the Raman intensity has a maximum when the incident polarization is parallel to the dimer axis – in fact, the angular variation can be quite well described by a $\cos^4(\alpha - \alpha_0)$ dependence, which is the expected variation if a "hot" gap site completely dominates the Raman response. For aggregates composed of more than two particles, the polarization dependence turned out to be in general more isotropic than for isolated dimers. Figure 5d shows a polar plot of the Raman intensity from spot C, which was composed of five Ag particles. In this case, a large signal was observed for all polarization angles, but with two noticeable anisotropic intensity peaks for polarization parallel to the 80°/260° and 160°/340° directions. We interpret such complicated polarization dependencies as a result of an entangled electromagnetic coupling between several particles. In this particular case, the angular variation indicates an interpretation in terms of a superposed signal from two dominating but perpendicular dimers within the five-particle aggregate. Figure 6 shows a GMT calculation that illustrates the variation in enhancement with polarization for a five-particle system (*not* chosen to mimic cluster C in Fig. 5). As expected, one finds that each polarization directions tend to "select" those gap sites for which the respective dimer axes overlap most with the incident polarization. However, the variation is not as clear-cut as for a symmetric dimer, simply because the total field at each gap site in a large low-symmetry cluster also involves retarded dipolar fields from distant particles that add to the local "dimer field" with varying phase factors.

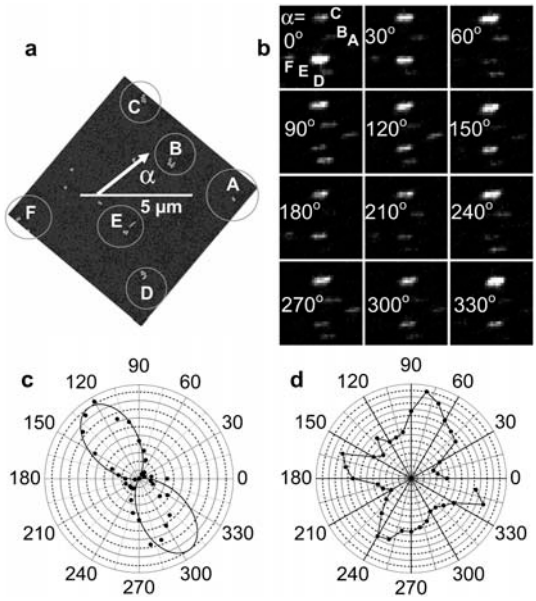

Fig. 5. (Reproduced from [6]), (**a**) SEM image of Hb/Ag clusters and (**b**) the corresponding polarized Raman images ($11 \times 11\,\mu m^2$) for different incident polarizations ($\lambda_I = 514.5\,nm$, $I_0 \approx 0.1\,W/\mu m^2$, Raman intensity integrated over a Stokes shift from $700\,cm^{-1}$ to $2200\,cm^{-1}$). The polar plots show the angular variation of the Raman intensity for (**c**) spot A and (**d**) spot C. The *full line* in (**c**) is a fit to a $\cos^4(\alpha - \alpha_0)$ dependence

3.3 Comparisons between Near-Field and Far-Field Spectra

In the preceding discussion, we have focused on the nano-optical phenomenon of greatest relevance to SERS, i.e., the near-field enhancement effect in Ag-particle aggregates. However, far-field optical properties, in particular extinction spectra, are often measured in conjunction with SERS experiments and it is therefore interesting to briefly compare the calculated near-field and far-field properties of Ag-particle aggregates. In Fig. 7, we do this for two different cases, a dimer and a low-symmetry pentamer. All gap sizes in both systems equals $d = 1\,nm$ but the spheres have different sizes in order to simulate the "nonideal" morphology of colloidal aggregates. In addition, the spheres have been positioned such that their lower boundaries form a plane, in order to simulate aggregates immobilized on a surface. As before, we compute near-field spectra for gap sites only.

In the case of the dimer, we first note the prominence of the aforementioned long-wavelength dipolar peak for polarization parallel to the dimer axis. This mode dominates both the intensity enhancement spectrum for the gap site and the far-field extinction spectrum, which in turn is composed mainly of elastic scattering. In addition, the short-wavelength region con-

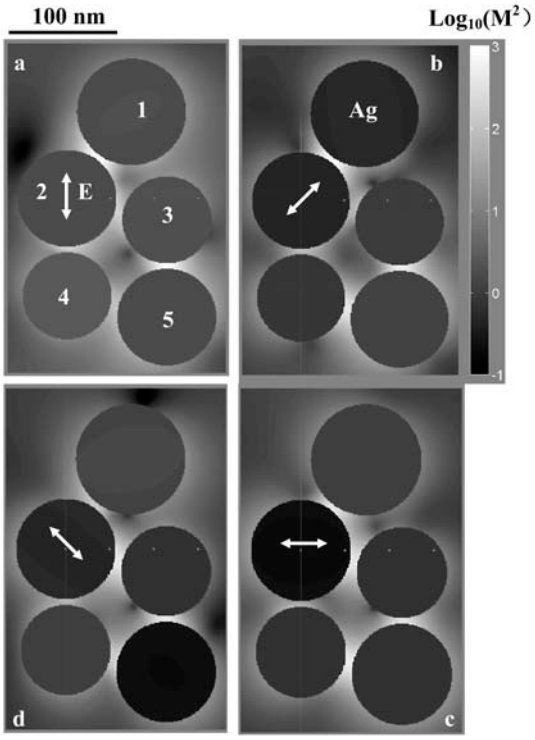

Fig. 6. (Adapted from [8]), Intensity enhancement factor M^2 (logarithmic scale) at 514.5 nm in a plane through the centers of five different Ag spheres with diameters $D_1 = 110\,\text{nm}$, $D_2 = D_5 = 100\,\text{nm}$ and $D_3 = D_4 = 90\,\text{nm}$. The gap dimensions are $d_{12} = d_{24} = d_{35} = 5.5\,\text{nm}$ and $d_{23} = d_{45} = 7.4\,\text{nm}$. The incident $\boldsymbol{k}$ vector is normal to the plane of the paper and arrows mark the different incident polarization vectors. The calculation is based on $N = 16$ multipoles and includes scattering orders up to $N_{\text{os}} = 200$

tains some well-defined modes that mainly originate in various hybridized quadrupolar resonances. When the polarization is turned perpendicular to the dimer axis, the enhancement at the gap site more-or-less vanishes, as before. The extinction spectrum is still dominated by a coupled dipolar mode, but its energy in this polarization configuration is such that it overlaps with higher-order multipolar peaks, and it does not contribute an enhancement at the gap site. All in all, there is clearly a reasonably good and understandable correspondence between far-field and near-field properties of the dimer. In the case of the pentamer, however, the situation is quite different. The extinction spectrum is dominated by a broad long-wavelength peak of dipolar origin, qualitatively similar to what is observed for strongly aggregated colloids. The near-field intensities in the junctions, in contrast, exhibit resonances that are much sharper than for the dimer and extremely polarization dependent. It is

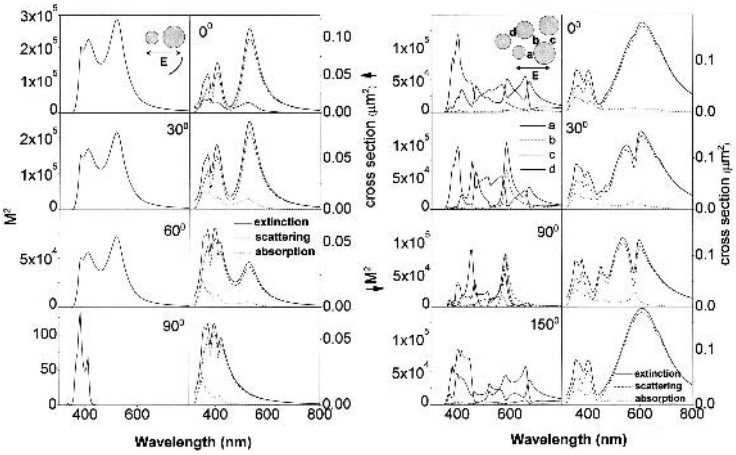

Fig. 7. Near-field intensity enhancement $M^2(\lambda)$ at "hot" gap sites and far-field cross sections (extinction, scattering, absorption) for a dimer ($D = 60\,\text{nm}$ and $D = 100\,\text{nm}$) an a pentamer ($D = 60\,\text{nm}$, $70\,\text{nm}$, $80\,\text{nm}$, $90\,\text{nm}$ and $100\,\text{nm}$) in vacuum with gap dimensions $d = 1\,\text{nm}$ throughout. The spheres are situated on a planar virtual surface and the incident $\boldsymbol{k}$ vector is normal to this surface with polarization as indicated in the insets. The calculations included multipoles up to order $N = 30$ and scattering processes up to infinite order through the matrix-inversion technique

possible that these resonances signal the onset of diffractive coupling effects caused by the coherent addition of fields emanating from distant particles. We note that similar effects, leading to high field enhancements, have been predicted and observed for both linear arrays of Ag particles [31, 32] and for large Au-particle clusters of fractal dimensions [33, 34]. Although the results require further analysis, the pentamer case thus illustrates that the near-field and the far-field properties of the same aggregate can be distinctly different. The results also indicate that the concept of "hot" junction sites that dominate the SERS response remains valid also for large particle aggregates of low symmetry. This is in qualitative agreement with experimental SERS studies of dense Ag particle layers, which exhibit single-molecule fluctuations even when analyte molecules are present at high concentrations [35, 36].

3.4 Including Molecular Quantum Dynamics into the EM SERS Theory

The electromagnetic mechanism of SERS discussed above treats the molecule as a "passive observer" of the field-enhancement effects. Recently, however, an extension of the em theory that includes a quantum optical description of a model molecule was put forward [9, 10, 11]. The model molecule is described by two electronic states (HOMO/LUMO) and one vibrational mode, and the

molecular dynamics is calculated using a density matrix approach, which allows one to compute absolute Raman, fluorescence and absorption cross sections and spectra for arbitrary irradiation levels. The parameters of the model were chosen so as to simulate the absorption spectrum of the fluorophore rhodamine 6G, which has become the work-horse of single-molecule SERS and fluorescence experiments (see, e.g., [36, 37]). The corresponding calculated energy integrated fluorescence cross section was found to be $\approx 10^{-16}\,\mathrm{cm}^2$, which agrees with experimental values for many fluorophores. The model molecule was then placed at a "hot" gap site with $d = 1\,\mathrm{nm}$ and $M^4 \approx 10^{10}$ and the combined Raman and fluorescence spectrum was calculated. The integrated SERS cross section was found to be $\approx 10^{-14}\,\mathrm{cm}^2$, i.e., two orders-of-magnitude higher than the fluorescence cross section of the free model-molecule and ~ 15 orders-of-magnitude higher than a "typical" Raman cross section of a nonresonant molecule ($\sigma_\mathrm{R} \approx 10^{-29}\,\mathrm{cm}^2$). These values are in agreement with recent single-molecule SERRS (surface-enhanced *resonance* Raman scattering) studies of rhodamine 6G [36,37], and suggest that no additional enhancement mechanisms beyond the "electromagnetic SERS theory" are needed in order to understand the single-molecule SERS phenomenon. Interestingly, the calculations also showed that a substantial enhanced fluorescence similar to the intense "SERS background" seen in many single-molecule SERRS experiments [36, 37] remained for a molecule in a "hot" gap site, whereas the familiar fluorescence-quenching effect dominated for molecules located near single particles.

3.5 Optical Forces

Optical forces has been a largely neglected aspect of SERS and nanoplasmonics in general, although it seems likely that such forces can be of both practical and fundamental importance. The total optical force that acts on a single particle or molecule situated in an inhomogeneous field can in general be resolved into two components: the gradient force and the dissipative force. In MKS units, we have:

$$\begin{aligned} \boldsymbol{F}_\mathrm{grad}(\boldsymbol{r}) &= \frac{n_\mathrm{m}}{2c}\Re\left\{\alpha(\lambda)\right\}\nabla I(\boldsymbol{r}) \\ \boldsymbol{F}_\mathrm{diss}(\boldsymbol{r}) &= \boldsymbol{k}\frac{n_\mathrm{m}}{c}\Im\left\{\alpha(\lambda)\right\} I(\boldsymbol{r})\,. \end{aligned} \tag{7}$$

Here, $\alpha(\lambda)$ is the wavelength-dependent dipole polarizability of the particle or molecule, n_m is the refractive index of the surrounding medium, c is the speed of light in vacuum and $I(\boldsymbol{r})$ is the optical intensity profile.

From (7), we see that the gradient force is repulsive when $\Re\{\alpha\} < 0$. This situation can occur for an incident wavelength on the blue side of a dipole resonance, such as a localized plasmon or molecular absorption band. For illumination on the red side of a resonance, on the other hand, the object is pulled towards regions of high local intensity, which is why dielectric objects

can be easily trapped using laser tweezers. The dissipative force, in contrast, is proportional to the extinction cross section $\sigma_{\text{ext}} = k\Im\{\alpha\}$ and therefore always positive, i.e., the object is pushed in the direction along the incident $\boldsymbol{k}$ vector.

From the discussions in preceding sections, we have seen that nanoparticle aggregates exhibit regions of ultrahigh field enhancement and at the same time regions where the optical field is not enhanced at all, or even excluded (see, e.g., the dark spots in Fig. 6). In [5], we examined whether the resulting intensity gradients could be large enough to actually pull molecules into the em "hot spots". Figure 8a shows the theoretical result for a linear trimer of Ag spheres, which exhibits its largest intensity enhancement $M^2 \approx 9.2 \times 10^5$ in the near-infrared ($\lambda_{\text{LSP}} \approx 760\,\text{nm}$). The molecular polarizability was chosen to mimic rhodamine 6G, which is resonant in the green ($\lambda_{\text{HOMO}\rightarrow\text{LUMO}} \approx 530\,\text{nm}$). The figure shows the conservative gradient force at $\lambda \approx 760\,\text{nm}$ in terms of the optical potential U in units of $k_{\text{B}}T$ at $T = 300\,\text{K}$ and for an incident intensity of $10\,\text{mW}/\mu\text{m}^2$, which is a rather typical excitation intensity in NIR SERS experiments. For the specific parameters used, the optical potential in the gap turns out to be $U \approx 6k_{\text{B}}T$. Thus, the optical force will be able to compete effectively with the random thermal motion of the molecule despite an irradiation wavelength far from the molecular resonance. Although no experimental verifications exists to date, it thus seems reasonable to believe that nanoscale optical forces acting on the molecular level could be of fundamental importance and, perhaps, be used to actively drive molecules to specific "hot spots" in plasmonic nanostructures. This is, however, not the only optical force effect that may be of relevance to SERS. In a recent experimental study, it was shown that the SERS intensity obtained from a colloidal solution of Ag particles covered by thiophenol could be increased dramatically if a high-intensity near-infrared laser beam was made to overlap with the green excitation laser in the Raman microscope [38]. This phenomenon was interpreted as the combined result of two effects: an accumulation of nanoparticles in the dual laser focus, i.e., the optical tweezers effect, and an optical aggregation of those nanoparticles due to electromagnetic interactions. The latter effect has been investigated theoretically in [5,39] and it is likely that it contributes to the plasmon renormalization recently observed when Ag particle dimers were created through optical manipulation [40].

The optical forces that act on a given particle due to the scattered fields from neighboring particles can be computed from Maxwell's stress tensor and represented in terms of an optical potential. An example is shown in Fig. 8b. The calculation is performed for a Ag-particle dimer illuminated by a beam of $\lambda = 514.5\,\text{nm}$ light polarized along the dimer axis and with a unit incident intensity of $1\,\text{mW}/\mu\text{m}^2$. The interparticle optical potential is shown as a function of gap size d for a few different sphere radii. For small distances, we find a strong attractive interaction, far greater than $k_{\text{B}}T$, that has a fairly long range, in particular for the larger particles. For longer sep-

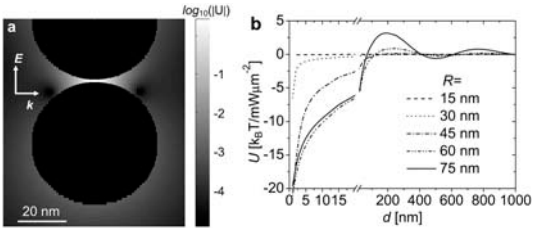

Fig. 8. (Adapted from [5]), (**a**) Spatial variation of the optical potential U in units of $k_{\mathrm{B}}T$ ($T = 300\,\mathrm{K}$) around a three-sphere system ($D = 50\,\mathrm{nm}$, $d = 1\,\mathrm{nm}$, $I_0 = 10\,\mathrm{mW}/\mu\mathrm{m}^2$) in water excited at 760 nm. The molecular polarizability was chosen to simulate rhodamine 6G. (**b**) Interparticle optical potential U $(d; R)$ for dimers in water in units of $k_{\mathrm{B}}T$ ($T = 300\,\mathrm{K}$) for an illumination intensity of $1\,\mathrm{mW}/\mu\mathrm{m}^2$, a wavelength of 514.5 nm and a polarization along the dimer axis

arations ($d \approx \lambda/2$) the interaction turns repulsive because the dipole fields of the individual particles are no longer in phase. The interaction is also repulsive for short separations if the incident field is polarized perpendicular to the dimer axis. The interparticle optical force can thus be expected to pull properly oriented particles together, creating "hot" gap sites, while aggregates that are oriented perpendicular to the incident polarization should be pushed apart. Experimental investigations in this direction are underway and will be reported elsewhere.

4 Summary

Using generalized Mie theory, it is possible to estimate field-enhancement effects in strongly interacting nanoparticle systems, including dense aggregates of several nanoparticles. Apart from the inherent approximation of a spherical particle shape, the method is a complete solution to Maxwell's equations. Based on GMT, we have shown that Ag nanoparticle aggregates exhibit polarization-dependent "hot" gap sites that will dominate the SERS response. This result is in agreement with the majority of SERS experiments and in line with previous theory results from the 1980s. The "hot" gap sites can be expected to yield SERS enhancements factors of the order of 10^{10} or above. When combined with a proper description of the quantum optical response of the molecule, this factor quantitatively explains SERS from single resonant molecules. We have also discussed optical forces in SERS and shown that molecules could be attracted to sites with high surface enhancement while properly aligned particles could be pulled closer together, even for relatively modest irradiation levels. These effects could be of both fundamental and practical importance.

References

[1] M. Moskovits: Rev. Mod. Phys. **57**, 783 (1985)
[2] H. X. Xu, et al.: Phys. Rev. Lett. **83**, 4357 (1999)
[3] H. X. Xu, et al.: Phys. Rev. E **62**, 4318 (2000)
[4] H. X. Xu, et al.: Proc. SPIE **4258**, 35 (2001)
[5] H. X. Xu, M. Käll: Phys. Rev. Lett. **89**, 246802 (2002)
[6] H. Xu, M. Käll: Chem. Phys. Chem. **4**, 1001 (2003)
[7] H. X. Xu: Phys. Lett. A **312**, 411 (2003)
[8] H. X. Xu: J. Opt. Soc. Am. **21**, 804 (2004)
[9] H. X. Xu, et al.: Phys. Rev. Lett. **93**, 243002 (2004)
[10] P. Johansson, H. X. Xu, M. Käll: Phys. Rev. B **72**, 035427 (2005)
[11] M. Käll, H. X. Xu, P. Johansson: J. Raman Spectrosc. **36**, 510 (2005)
[12] G. Mie: Ann. Phys. **25**, 377 (1908)
[13] P. K. Aravind, A. Nitzan, H. Metiu: Surf. Sci. **110**, 189 (1981)
[14] P. K. Aravind, H. Metiu: Surf. Sci. **124**, 506 (1983)
[15] P. K. Aravind, H. Metiu: J. Phys. Chem. **86**, 5076 (1982)
[16] J. I. Gersten: J. Chem. Phys. **72**, 5779 (1980)
[17] J. I. Gersten, A. Nitzan: J. Chem. Phys. **73**, 3023 (1980)
[18] M. Inoue, K. Othtaka: J. Phys. Soc. Jpn. **52**, 3853 (1989)
[19] P. C. Waterman: Phys. Rev. D **3**, 825 (1971)
[20] M. I. Mischenko, et al.: J. Quantum Spectrosc. Radiat. Transfer **88**, 357 (2004)
[21] S. Stein: Quart. Appl. Math. **19**, 15 (1961)
[22] O. R. Cruzan: Quart. Appl. Math. **20**, 33 (1962)
[23] A. K. Hamid, I. R. Ciric, M. Hamid: IEEE Proc. H **138**, 565 (1991)
[24] Y. M. Wang, W. C. Chew: IEEE Trans. Antennas Propag. **41**, 1633 (1993)
[25] K. A. Fuller: Appl. Opt. **30**, 4716 (1991)
[26] J. A. Stratton: *Electromagnetic Theory* (McGraw-Hill, New York 1941)
[27] P. B. Johnson, R. W. Christy: Phys. Rev. B **6**, 4370 (1972)
[28] L. Gunnarsson, et al.: J. Phys. Chem. B **109**, 1079 (2005)
[29] A. Liebsch: *Electronics Excitations at Metal Surfaces* (Plenum, New York 1997)
[30] A. Pack, M. Hietschold, R. Wannemacher: Opt. Comm. **194**, 277 (2001)
[31] S. Zou, N. Janel, G. C. Schatz: J. Chem. Phys. **120**, 10871 (2004)
[32] E. M. Hicks, et al.: Nano Lett. **5**, 1065 (2005)
[33] V. P. Drachev, et al.: *Nonlinear Optical Effects and Selective Photomodification of Colloidal Silver Aggregates* (Springer, Berlin, Heidelberg, New York 2002) p. 113
[34] E. J. Bjerneld, P. Johansson, M. Käll: Single Mol. **1**, 239 (2000)
[35] E. J. Bjerneld, et al.: J. Phys. Chem. A **108**, 4187 (2004)
[36] S. M. Nie, S. R. Emory: Science **275**, 1102 (1997)
[37] K. A. Bosnick, J. Jiang, L. E. Brus: J. Phys. Chem. B **106**, 8096 (2002)
[38] F. Svedberg, M. Käll: Faraday Discuss. **132**, 35 (2006)
[39] A. J. Hallock, P. L. Redmond, L. E. Brus: Proc. Natl. Acad. Sci. **102**, 1280 (2005)
[40] J. Prikulis, et al.: Nano Lett. **4**, 115 (2004)

Index